First-principles study of water adsorption and a high-density interfacial ice structure on (1×1)-O/Rh(111)

C. Thierfelder* and W. G. Schmidt
Lehrstuhl für Theoretische Physik, Universität Paderborn, 33095 Paderborn, Germany
(Received 31 May 2010; revised manuscript received 10 July 2010; published 2 September 2010)

The adsorption of water monomers, small water clusters, and water thin films on (1×1)-O/Rh(111) surfaces is studied by density-functional theory. The calculations give a microscopic interpretation for the high-density ice phase detected experimentally on the surface [K. D. Gibson, M. Viste, and S. J. Sibener, J. Chem. Phys. **112**, 9582 (2000)].

DOI: 10.1103/PhysRevB.82.115402 PACS number(s): 68.08.Bc, 68.43.Fg, 82.30.Rs

It is well known that water interacts weakly with transition-metal surfaces with an interaction strength comparable to the water-water, i.e., hydrogen bonding.[1–3] Recently, the increased capability of surface scientists to probe at the molecular level has resulted in more detailed information concerning the properties of adsorbed water molecules on metal surfaces.[4]

The interaction of water with ruthenium has found interest because of the fact that water wets Ru(0001) by forming a half-dissociated H-bonding network.[5] This induced interest in the growth process of water layers and crystalline ice on Rh(111).[6–8] The presence of subsurface oxygen and of a surface oxide significantly alters the physical and chemical properties of metal surfaces.[9] Gibson *et al.*[10] report a particularly interesting finding in that context. They found a novel high-density form of interfacial ice on top of (1×1)-O/Rh(111). In this study, we aim to elucidate this finding from first-principles calculations.

A traditional structural model for water-metal interaction has been based on the basal plane of ice Ih, a tetrahedral arrangement of water molecules arranged in buckled hexagonal rings; thus, this model is called an icelike bilayer. This model was originally proposed for the first water layer on Ru(0001) (Ref. 11) because of the close match between lattice constants: 4.50 Å for the a lattice constant of bulk hexagonal ice Ih, near 100 K and 4.68 Å for Ru(0001). Rh(111) actually has an even more favorable lattice constant, the $(\sqrt{3}\times\sqrt{3})R30°$ dimension being 4.66 Å.

The calculations are performed using density-functional theory (DFT) within the generalized gradient approach (GGA) as implemented in the Vienna *ab initio* simulation package (VASP).[12,13] The electron-ion interaction is described by the projector-augmented wave scheme.[14] The electronic wave functions are expanded into plane waves up to a kinetic energy of 30 Ry.

The surface is modeled by periodically repeated slabs. Each supercell consists of four rhodium layers where the lowest is fixed in bulk position, the oxygen layer as well as a vacuum region equivalent to six layers. The three uppermost layers as well as the oxygen layer and the admolecule degrees of freedom are allowed to relax until the forces on the atoms are below 5 meV/Å. The Brillouin-zone (BZ) integration was approximated by a sum over a regular Γ-centered mesh of (4×4×1) **k** points for surface calculations.

As the description of hydrogen bonds is sensitive with respect to the exchange-correlation (XC) functional it is necessary to evaluate the performance of different functionals for ice as well as rhodium. Using the Perdew and Wang (PW91) and Perdew, Burke, and Ernzerhof (PBE) functionals[15,16] for bulk ice, the obtained results for the sublimation energy, equilibrium volume, and bulk modulus are in very good agreement with experiment, as shown in previous studies.[17,18]

We performed rhodium bulk (fcc) calculations using a unit cell containing three atoms and a mesh of (4×4×4) **k** points in the irreducible part of the BZ. These calculations result in a cohesive energy of 6.05 eV per atom for the PW91 functional, somewhat above the experimental value of 5.75 eV.[19] The PW91 equilibrium lattice constant 3.823 Å is about 0.6% larger than the experimental value of 3.80 Å. Because the PBE and PW91 functionals lead to almost identical results, PW91 is used throughout the rest of this work.

At first the chemisorption of oxygen atoms on Rh(111) is investigated. To find the global minimum of the oxygen adsorption site, a potential-energy surface (PES) for a single oxygen atom is calculated. Apart from the lateral position of the adsorbate oxygen, the structural degrees of freedom of both substrate and adsorbate were fully relaxed in these calculations. The calculated data are shown in Fig. 1.

As we use a fine mesh we are sure to find all local minima. Here the PES exhibits three local minima. The first one is very shallow and above a top-layer rhodium atom. The other two minima are about 0.8 eV lower in energy and located at fcc- or hcp-hollow sites of the rhodium substrate. The fcc-hollow site is 0.2 eV lower than the hcp site and builds therefore the most favorable adsorption position with

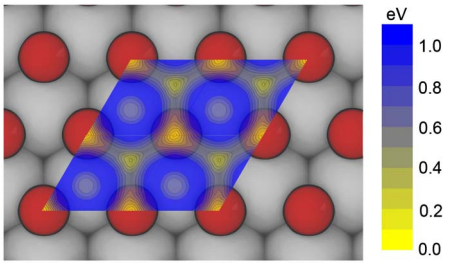

FIG. 1. (Color online) Potential-energy surface for a single oxygen atom on Rh(111). Oxygen (rhodium) atoms are represented by red (gray) balls

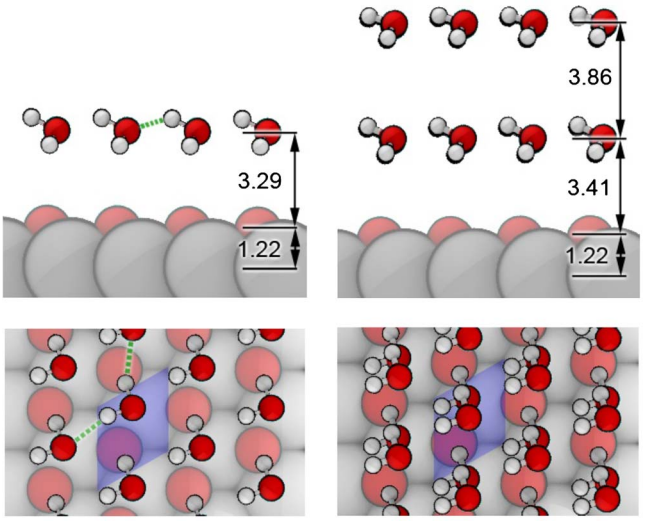

FIG. 2. (Color online) Schematic top and side view of adsorption structures C1×1-S (left) C1×1-D (right). The hydrogen bonds are only depicted on the left-hand side by green dashed lines.

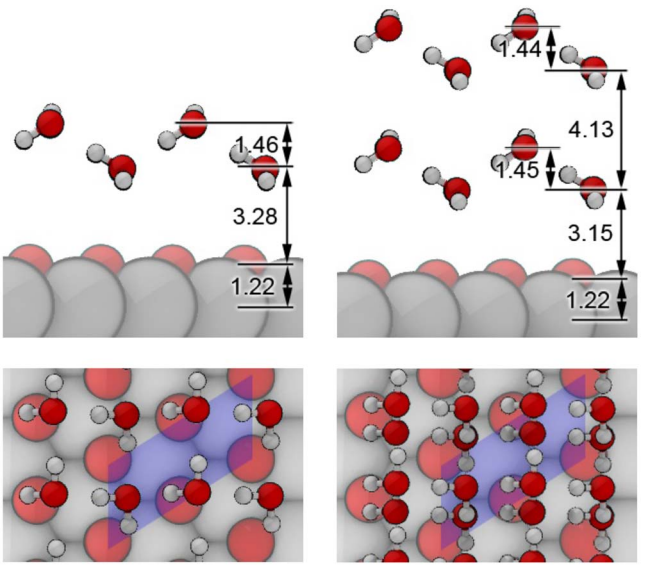

FIG. 3. (Color online) Schematic top and side view of adsorption structures C2×1-S (left) C2×1-D (right).

an adsorption energy of 4.41 eV. A full relaxation of the structure leads to a oxygen-rhodium interlayer spacing $d_{\text{O-Rh}}$ of 1.22 Å. A mean outermost substrate interlayer spacing of 2.37 Å is found which is extended relative to the corresponding value for the clean surface. The interlayer spacing decreases then slowly toward the bulk value of 2.21 Å. This results are in good agreement with an earlier theoretical study by the Scheffler group.[20]

As we aim to find the proposed high-density ice phase,[10] we start with the investigation of configurations of high water coverages and decrease it step by step. First, the adsorption of a single water molecule on the (1×1) surface unit cell was studied. Again a PES was calculated but in order to account for the fact that energy barriers hinder the free rotation of surface adsorbed water molecules, the minimum-energy geometry for every PES sampling point was obtained by probing three different molecular starting orientations, i.e., (i) one O-H bond pointing downward, (ii) the C_2 axis perpendicular to the surface, and (iii) the water molecule parallel to the surface. Only one favorable adsorption site was found and a full relaxation lead to adsorption configuration C1×1-S (S single), showed in Fig. 2. The admolecule is oriented almost parallel to the surface. One hydrogen is pointing slightly downward, forming a hydrogen bond (1.95 Å) with a neighboring water molecule. The second hydrogen is pointing in plane toward another neighboring water molecule forming a second hydrogen bond (1.89 Å), indicated in Fig. 2 by dashed lines. These values are well within common geometrical boundaries for hydrogen bonds.[21,22] The relatively large distance of the ice layer to the surface (3.29 Å) indicates that no direct bonding is occurring and can be explained trough the stabilization of the ice monolayer by the surface. The adsorption energy per water molecule is 0.21 eV.

Starting with this configuration and increasing the coverage to two molecules leads to the formation of a second ice layer of the similar structure to the first one. This configuration is denoted by C1×1-D (D double) and depicted on the right-hand side in Fig. 2. The distance of the first layer to the surface is slightly increased (3.41 Å) with respect to C1×1-S and the distance between the two ice layers is 3.86 Å. Both layer also differ by their lateral position. We also note a small decrease in the adsorption energy per admolecule to 0.20 eV.

Increasing the coverage by a third water molecule in surface unit cell results in configuration with a third ice layer (C1×1-T). The fact that the binding energy per admolecule is again 0.20 eV indicates the beginning of the growth of solid ice on top of the surface.

In the next step we used a (2×1) surface unit cell to relax the geometry constrains given by the periodic boundary conditions. The relaxation of the structure C1×1-S leads to structure C2×1-S (Fig. 3). The most notable difference to configuration C1×1-S is the formation of an ice Ih-like bilayer structure with a bilayer distance of 1.46 Å which is about 71% larger compared to hexagonal ice.[17] The distance of the bilayer to the surface is not changed. Another interesting fact is that the OH group of water molecule in the upper bilayer has changed its orientation by rotating 180° around the axis of the remaining OH group. These changes in the adsorption geometry result in a substantial increase in the adsorption energy of 0.57 eV/molecule.

Increasing the coverage resulted again in the formation of more ice bilayers and the configurations are subsequently denoted by C2×1-D (Fig. 3) and C2×1-T. The distance between different bilayers is about 4.13 Å and deviates only slightly for higher coverages while the thickness of the bilayer remains unchanged at 1.45 Å. Also the adsorption energies per molecule decreased only by 0.02 eV and 0.03 eV, respectively (Table I). But while in hexagonal ice the oxygen of two neighboring bilayers express a mirror symmetry (Fig. 4) here the bilayers appear simply stacked onto each other. To ensure that a stable minimum-energy structure was indeed found, larger surface unit cells of (2×2) and (4×1) translational symmetry were utilized. This did not result, in how even more favorable adsorption geometries.

TABLE I. Results for the lattice constant, bulk modulus, and cohesive energies of rhodium bulk for different XC functionals.

	a_0 (Å)	B (Mbar)	E_{coh} (eV/atom)
LDA	3.605	2.79	7.49
PBE	3.831	2.42	6.02
PW91	3.836	2.52	6.05
Expt.[a]	3.80	2.69	5.75

[a]Reference 19.

Removing one water molecule from C2×1-S, results in adsorption structure C2×1-H. The binding energy of the remaining admolecule of 0.37 eV is 0.20 eV less then in C2×1-S. For a (3×3) surface unit cell we found a stable configuration containing six water molecules, denoted by C3×3 (Fig. 4). Interestingly an ice bilayer is formed which is quite similar to hexagonal ice, favored by the close match of the respective surface lattice constants. In contrast to the previously discussed configurations, C3×3 shows hydrogen atoms pointing downward toward the surface oxygen. The hydrogen bonds are indicated in Fig. 4. Notable differences to the ice Ih bilayer include the smaller bilayer thickness of 0.57 Å and that opposite sides of the hexagons have lengths of 2.63 and 2.83 Å.

Then the cell size was further enlarged to (4×4). In the case of six water molecules contained in the cell, water hexamers are formed, which are well known from other water-metal interfaces[23] for this coverages.[3] They are as well hydrogen bonded to the surface with a binding energy of 0.23 eV/molecule, Fig. 5.

The lowered coverage studied here was realized by considering single water molecules within a (2×2) surface unit cell. Because only bonds to the substrate can be established, the adsorption energy drops to 0.09 eV per monomer.

Table II summarizes the adsorption energies for all considered structures. The energies as well as our error estimates

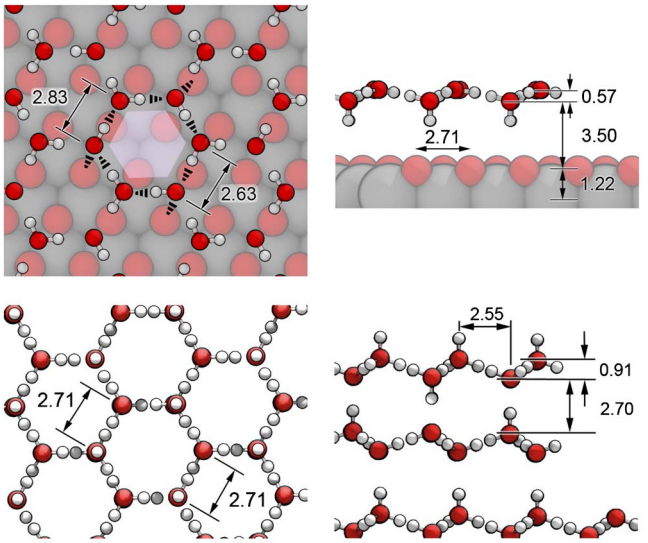

FIG. 4. (Color online) Schematic top and side view of adsorption structure C3×3 (top) and ice Ih (bottom).

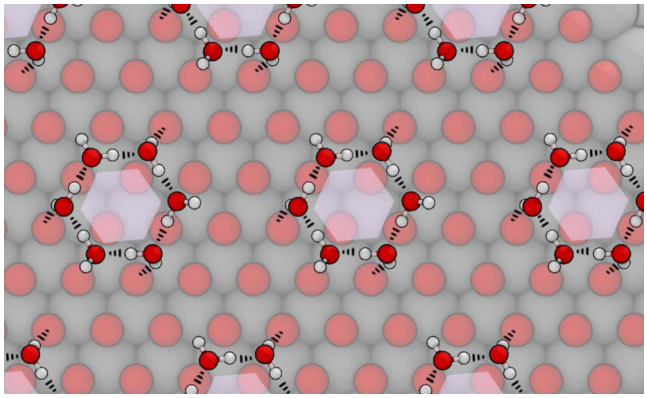

FIG. 5. (Color online) Schematic top and side view of adsorption structure C4×4.

are also shown in Fig. 6. For each adsorption geometry given, several calculations were made by using decent starting geometries, which are sufficiently distributed in the configuration space. As most of the calculations converge to the same structure we are rather sure, that all given geometries are true global minimum structures.

The adsorption energy per water molecule for the various adsorption configurations are depicted in Fig. 6. It can be seen that the configuration C2×1-S is the energetically most stable one. Increasing the number of ice layers does not alter the adsorption energy significantly. The C1×1-S/D/T configurations with the same coverages are clearly less favorable. The investigated low coverage species show an almost linear dependence on the coverage.

In order to compare energetically the adsorption models with different water coverages, the thermodynamic grand-canonical potential,

$$\Omega(\mu_{H_2O}) = \frac{1}{A}[F_{surf}(n) - n\mu_{H_2O}] \approx \frac{1}{A}[E_{surf}(n) - n\mu_{H_2O}] \tag{1}$$

needs to be calculated, where $F_{surf}(n)$ is the surface free energy which we approximate by the total surface energy

TABLE II. Summary of all discussed adsorption configurations.

Coverage (Å^{-2})	Configuration	Ads. energy per molecule (eV)
0.47	C2×1-T	−0.54
0.47	C1×1-T	−0.20
0.32	C2×1-D	−0.55
0.32	C1×1-D	−0.20
0.16	C2×1-S	−0.57
0.16	C1×1-S	−0.21
0.11	C3×3	−0.50
0.08	C2×1-H	−0.37
0.06	C4×4	−0.23
0.04	C2×2	−0.09

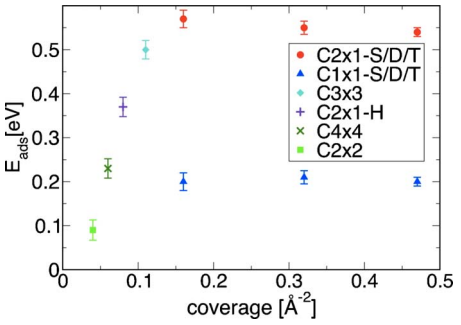

FIG. 6. (Color online) Calculated adsorption energy per water molecule vs coverage.

$E_{\mathrm{surf}}(n)$ at zero temperature, assuming similar entropy contributions for different adsorption configurations. The number of adsorbate molecules is represented by n. Figure 7 shows the resulting phase diagram in dependence on the water chemical potential $\mu_{\mathrm{H_2O}}=\partial U/\partial n_{\mathrm{H_2O}}$. Here two important values are indicated. The difference between $\mu^{\mathrm{gas}}_{\mathrm{H_2O}}$ and $\mu^{\mathrm{ice}}_{\mathrm{H_2O}}$ is equivalent to the binding energy of a water molecule in bulk ice Ih. Extreme water-rich conditions are marked by a vertical line denoted $\mu^{\mathrm{solid}}_{\mathrm{H_2O}}$. This value corresponds to a (1×1)-O/Rh(111) surface in equilibrium with bulk water, approximated here by calculations for ice Ih.[17] Lower values of μ indicate an increasingly dry environment. The zero-temperature calculation for gas-phase water molecules $\mu^{\mathrm{gas}}_{\mathrm{H_2O}}$ is indicated by another vertical line.

As expected, the clean (1×1)-O/Rh(111) surface is stable for low values of the water chemical potential. As the environment gets more and more humid, a variety of water-adsorbed surface structures may be observed. The adsorption models C2×1-S and C2×1-D are stable for a very small window of preparation conditions, while C2×1-T, the adsorption of the third bilayer is stable for a relatively wide range of water-rich and extreme water-rich conditions. For higher coverages one expects the growth of more bilayers, i.e., the growth of bulk ice.

The adsorption model C2×1-S is likely to correspond to the proposed (2×1) high-density interfacial ice structure observed by Gibson *et al.*[10] The surface density of our (2×1) ice bilayer (0.158 Å^{-2}) is about 33% higher than the density

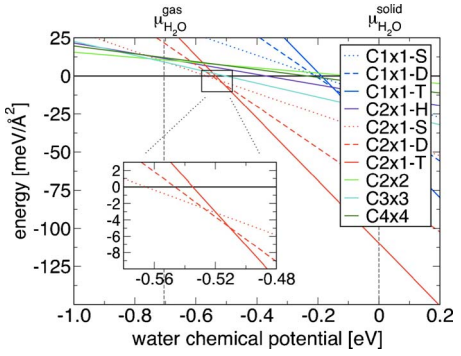

FIG. 7. (Color online) Calculated phase diagram of the (1×1)-O/Rh(111) surface in dependence on the water chemical potential given with respect to ice Ih.

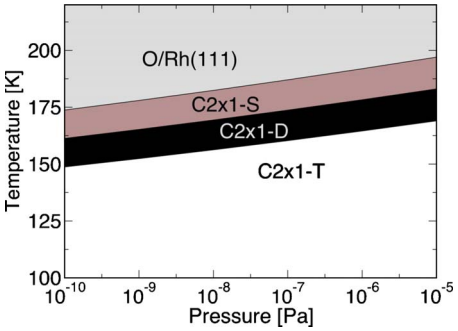

FIG. 8. (Color online) Calculated phase diagram of the (1×1)-O/Rh(111) surface in dependence on the water chemical potential given with respect to ice Ih.

of an ice Ih bilayer (0.118 Å^{-2}) which means that it is indeed a high-density structure.

In order to relate the water chemical potential to the experimental conditions in terms of pressure and temperature, we calculate the chemical potential in the approximation of a polyatomic ideal gas,[24]

$$\Delta\mu_{\mathrm{H_2O}}(p,T)=k_{\mathrm{B}}T\left[\ln\left(\frac{p\lambda^3}{k_{\mathrm{B}}T}\right)-\ln(Z_{\mathrm{rot}})-\ln(Z_{\mathrm{vib}})\right], \quad (2)$$

where k_{B} is the Boltzmann constant, T the temperature, p the pressure, $\lambda=\sqrt{h^2/2\pi mk_{\mathrm{B}}T}$ the de Broglie thermal wavelength of the water molecule, and

$$Z_{\mathrm{rot}}=\frac{\sqrt{\pi I_1I_2I_3}(2k_{\mathrm{B}}T)^{3/2}}{\sigma\hbar^3}, \quad (3)$$

$$Z_{\mathrm{vib}}=\prod_{\alpha}\left[1-\exp\left(-\frac{\hbar\omega_\alpha}{k_{\mathrm{B}}T}\right)\right]^{-1}, \quad (4)$$

its rotational and vibrational partition functions, respectively. The I_i are the momenta of inertia of the water molecule and ω_α the vibrational frequencies. Our results are in good agreement with the JANAF data[25] for the pressure values tabulated. The calculated pressure- and temperature-dependent phase diagrams of the water-(1×1)-O/Rh(111) system is shown in Fig. 7.

At temperatures above 175 K the clean (1×1)-O/Rh(111) surface is stable. By decreasing the temperature a first adsorbed water layer becomes stable over a wide range of the water partial pressure. A further lowering of the temperature leads to a rapid growth of several bilayers, Fig. 8.

The experimental conditions reported for the growth of the first ice layer are a temperature of 120 K and a pressure of 10^{-8} Pa.[10] This deviates some what (≈40 K) from our calculations, possibly related to the approximations entering the calculations such as the neglect of van der Waals bonding, as well as the fact that the experimental results were not necessarily obtained at thermodynamic equilibrium.

To summarize, DFT-GGA calculations for water adsorbed on the oxygen-adsorbed Rh(111) surface were performed. Among the different adsorption configurations which were discussed we found a high-density (2×1) interfacial ice

layer. It exhibits some similarities to ice Ih and explains the experimental finding by Gibson *et al.*[10] The adsorption temperature of 175 K obtained from a thermodynamical stability analysis fits reasonably well the experimental value of 120 K.

Financial support from the DFG as well as grants of supercomputer time by the Höchstleistungsrechenzentrum Stuttgart and the Paderborn Center for Parallel Computing PC^2 are gratefully acknowledged.

*c.thierfelder@uni-paderborn.de

[1] P. A. Thiel and T. E. Madey, Surf. Sci. Rep. **7**, 211 (1987).
[2] A. Verdaguer, G. Sacha, H. Bluhm, and M. Salmeron, Chem. Rev. **106**, 1478 (2006).
[3] A. Michaelides and K. Morgenstern, Nature Mater. **6**, 597 (2007).
[4] S. Schnur and A. Groß, New J. Phys. **11**, 125003 (2009).
[5] P. J. Feibelman, Science **295**, 99 (2002).
[6] P. J. Feibelman, Phys. Rev. Lett. **90**, 186103 (2003).
[7] A. Beniya, S. Yamamoto, K. Mukai, Y. Yamamashita, and J. Yoshinobu, J. Chem. Phys. **125**, 054717 (2006).
[8] A. Beniya, Y. Sakaguchi, T. Narushima, K. Mukai, Y. Yamamashita, S. Yoshimoto, and J. Yoshinobu, J. Chem. Phys. **130**, 034706 (2009).
[9] K. A. Peterlinz and S. J. Sibener, J. Phys. Chem. **99**, 2817 (1995).
[10] K. D. Gibson, M. Viste, and S. J. Sibener, J. Chem. Phys. **112**, 9582 (2000).
[11] D. L. Doering and T. E. Madey, Surf. Sci. **123**, 305 (1982).
[12] G. Kresse and J. Furthmüller, Comput. Mater. Sci. **6**, 15 (1996).
[13] G. Kresse and D. Joubert, Phys. Rev. B **59**, 1758 (1999).
[14] P. E. Blöchl, Phys. Rev. B **50**, 17953 (1994).
[15] J. P. Perdew, J. A. Chevary, S. H. Vosko, K. A. Jackson, M. R. Pederson, D. J. Singh, and C. Fiolhais, Phys. Rev. B **46**, 6671 (1992).
[16] J. P. Perdew, K. Burke, and M. Ernzerhof, Phys. Rev. Lett. **77**, 3865 (1996).
[17] C. Thierfelder, A. Hermann, P. Schwerdtfeger, and W. G. Schmidt, Phys. Rev. B **74**, 045422 (2006).
[18] C. Thierfelder and W. G. Schmidt, Phys. Rev. B **76**, 195426 (2007).
[19] C. Kittel, *Introduction to Solid State Physics*, 7th ed. (Wiley, New York, 1996).
[20] M. V. Ganduglia-Pirovano and M. Scheffler, Phys. Rev. B **59**, 15533 (1999).
[21] E. Schwegler, G. Galli, and F. Gygi, Phys. Rev. Lett. **84**, 2429 (2000).
[22] P. Wernet *et al.*, Science **304**, 995 (2004).
[23] S. Wippermann and W. G. Schmidt, Phys. Rev. B **78**, 235439 (2008).
[24] L. D. Landau and E. M. Lifshitz, *Statistical Physics, Part I*, 3rd ed. (Butterworth Heinemann, Oxford, 1981).
[25] D. R. Stull and H. Prophet, *JANAF Thermochemical Tables*, 2nd ed. (U.S. NBS, Washington, D.C., 1971).